Progress in Propulsion Physics **8** (2016) 283-306
DOI: 10.1051/eucass/201608283

THEORETICAL PREDICTION OF REGRESSION RATES IN SWIRL-INJECTION HYBRID ROCKET ENGINES

K. Ozawa[1] and T. Shimada[2]

[1]University of Tokyo, Department of Aeronautics and Astronautics
3-5-1 Yoshinodai, Chuo-ku, Sagamihara 252-5210, Japan
[2]Japan Aerospace Exploration Agency (JAXA)
Institute of Space and Astronautical Science
3-5-1 Yoshinodai, Chuo-ku, Sagamihara 252-5210, Japan

The authors theoretically and analytically predict what times regression rates of swirl injection hybrid rocket engines increase higher than the axial injection ones by estimating heat flux from boundary layer combustion to the fuel port. The schematic of engines is assumed as ones whose oxidizer is injected from the opposite side of the nozzle such as ones of Yuasa *et al.* propose. To simplify the estimation, we assume some hypotheses such as three-dimensional (3D) axisymmetric flows have been assumed. The results of this prediction method are largely consistent with Yuasa's experiments data in the range of high swirl numbers.

NOMENCLATURE

a	constant related to regression rate
B	blowing parameter: $B_z \equiv (\rho u_r)_w u_{ze}/\tau_{zw}$; $B_\theta \equiv (\rho u_r)_w u_{\theta e}/\tau_{\theta w}$
B_t	thermodynamic chemical blowing parameter: $B_t \equiv u_{e_z}\Delta h/(u_{b_z} h_\nu)$ (in quasi-steady codition, equal to B_z)
c_f	skin-friction coefficient in axial flow: $c_{f_z} = \tau_{rz_w}/(\rho u_{z_e}/2)$; $c_{f_\theta} = \tau_{r\theta_w}/(\rho u_{\theta_e}/2)$
c_p	specific heat at constant pressure
C	specific heat of solid fuels
C_H	Stanton number
D	port diameter
G_o	oxidizer mass flux
Δh	enthalpy difference between flame sheet and port surface
h_ν	total enthalpy of solid fuel gasification at ambient temperature
k	blocking exponent in axial flows
k'	blocking exponent in swirl flows

l mixing length tensor
L port length
n mass flux exponent for hybrids
p exponent related to swirl decay in cold flows $p = -0.569\mathrm{Re}_D^{-0.277} D^{-1}$
P pressure
q constant used for approximation of the function of blowing parameter in axial flows
q' constant used for approximation of the function of blowing parameter in swirl flows
q_r radial direction heat flux
$\dot{Q}_c$ heat flux to the wall
r radial location
$\dot{r}$ regression rate
S swirl number
t time
T temperature
u velocity
z axial location
α_z constant related to approximation of C_{f_z}
β_z constant related to approximation of C_{f_z}
γ_z exponent related to approximation of C_{f_z}
δ boundary layer thickness
ε perturbation scale
η nondimensional height in boundary layer
θ angle
κ constant related to mixing length
μ average gas viscosity
ν average gas kinematic viscosity
ξ swirl strength: $\xi/2 \approx S$
ρ density
τ shear stress
φ nondimensional velocity in boundary layer
ω angular velocity
$\overline{\omega}$ nondimensional angular velocity: $\overline{\omega} = (R - \delta_\theta)\omega / u_{\theta_e}$

Subscripts

b flame area
bl boundary layer
e free stream or main flow
f fuel
o oxidizer
r radial direction
ref reference point
w wall

z axial direction
θ angular direction
ξ in cases with swirl
$\bar{}$ nondimensionalized
$\cdot$ time differential

1 INTRODUCTION

Hybrid propulsion is expected to be applied for various purposes like space transportation, space tourism, and space education because of its inherent safety and low cost. In conventional hybrid rocket engines, liquid oxidizer is injected into a combustion chamber that contains solid fuel such as hydroxyl-terminated polybutadiene (HTPB) (which is a binder for solid rocket motors). Gasified oxidizer and fuel combust in the boundary layer over the fuel-port wall surface. Hybrid rockets using HTPB have been developed for many years, but as the regression rate of such rockets is low (up to 1 mm/s at the oxygen mass flux below 100 kg/(m^{2}s)), they seem to have no bright future, i. e., they are at a dead end [1]. That is why multiport systems are required in the practical use of hybrid engines using HTPB. However, such systems decrease launch capability from potential one because of remnants of the fuel in multiport engines and have an anxiety of the drop of them around the end times of combustion.

To solve this problem, swirl injection (or vortex injection) method is proposed as a way to realize higher regression rates without energetic additives or the change of fuels [2, 3]. This method is to inject liquid oxidizer that has swirl velocity components. The characteristics of this injection method is that the radial pressure gradient caused by swirl makes the flame area in the boundary layer closer to the wall of the fuel port. This effect increases the amount of heat transfer from the flame area to the wall and, therefore, higher regression rates can be achieved. Lab-scale swirl-injection hybrid rocket motors have been developed by several researchers (see, for example, Knuth *et al.* [2], Yuasa *et al.* [3]) who proved the increase of regression rates. However, there have been few studies which theoretically and quantitatively predict the increase of regression rates by swirl. They are useful for designing engines of different scale, for better understanding of various phenomena in engines, and as an alternative way to estimate the effects of swirl strength on the regression rate and other properties. Furthermore, theoretical and analytical studies are flexible in the sence that they are not subject to practical limitations such that a variable is intrinsically independent on other variables, but in actual experiments, such dependence exists because of experimental equipment and conditions. For this reason, theoretical approaches can reveal hidden properties of a phenomenon while experimental approaches cannot. Moreover, current computational fluid dynamics (CFD) approaches do not always accurately simulate actual swirl flows, and the techniques of swirl flow simulation in CFD are under development [4]. That is why, it is important

to construct the theoretical analytical approach for predicting regression rates in swirl-injection hybrid rockets.

The purpose of this paper is to extend the estimation method of regression rates developed for axial hybrid rocket engines to engines with swirl injection. To predict regression rates, one should estimate the heat flux to the fuel port based on some already known quantities which represent the flow field and other parameters in the combustion chamber using the following equation at quasi-steady state:

$$\dot{Q}_c = \rho_f \dot{r} h_\nu \tag{1}$$

where ρ_f and h_ν depend on fuel species and ambient temperature (h_ν includes the amount of specific heat to gasify the fuel at the ambient temperature). Thus, if one has another expression for Q_c, the regression rate $\dot{r}$ can be readily estimated. In 1960s, Marxman and Gilbert [5,6] conducted theoretical and analytical studies on boundary layer combustion and evaluated heat transfer to the fuel surface in axial hybrid motors. Their approach starts from the relationship between the heat transfer and the skin-friction suggested by Lees [7]. This relationship means that if the skin-friction with fuel blowing from the wall can be estimated, it is possible to estimate the heat flux to the wall. Their approach to evaluate the shear stress at the wall with fuel blowing was in expressing it through the simple relationship without fuel blowing given by an empirical formula.

In the present study, the authors first added some hypotheses needed to simplify the problem and to evaluate the effects of circumferential flows, and extended the flow field to the 3D axisymmetric pattern. However, the concept of the approach to evaluate the heat flux of swirl-injection hybrids remains the same as that of previous studies in terms of the introduction of Reynolds analogy and the connection with the shear stress at the wall. When Reynolds analogy is considered, one has to keep in mind that the similarity between temperature and velocity fields is applied to the axial component of the velocity vector rather than to the velocity vector itself. Then, the authors made an attempt to evaluate the axial component of the shear stress at the wall in swirl flows with fuel blowing with those without fuel blowing. On the way of the evaluation, the flow field in the boundary layer with swirl and without fuel blowing was used to study the effects of swirl and blowing separately. Eventually, regression rates in swirl-injection hybrids were theoretically derived and their predicted values were compared with the experimental results of Yuasa *et al.* [3].

2 MODELING AND HYPOTHESES OF FLOWS IN SWIRL-INJECTION HYBRID ROCKET ENGINES

First of all, let us consider 10 hypotheses related, mainly, to the flow field. These can largely be classified into two types. The assumptions of the first type

Table 1 The hypotheses on swirl flows

No.	Hypotheses
1	Flow in the combustion chamber is axisymmetric
2	Prandtl number in the flow is 1
3	Flow in the boundary layer is incompressible
4	Axial velocity components are uniform in axial and radial directions except for the boundary layer over the fuel-port wall surface
5	Circumferential velocity distribution is the same as rigid-body rotation in the radial direction except for the boundary layer over the fuel-port wall surface
6	Axial velocity components in the boundary layer obey the power law when there is no blowing from solid fuel
7	Circumferential angular velocity components in the boundary layer obey the power law when there is no blowing from solid fuel
8	Swirl without fuel blowing from the solid fuel decays exponentially to the axial direction
9	Thickness of axial boundary layer is larger than that of the circumferential one
10	Heat flux to the fuel port by heat convection is much larger than the one by radiation

are the assumptions taken from the theory of Marxman *et al.* to simplify the complex flow in combustion chambers. The assumptions of the second type are the newly added assumptions adopted to simplify the handling swirl flows and corresponding to the features observed in experiments related to swirl flows. All hypotheses assumed in this paper are summarized in Table 1. These hypotheses are adopted for the engines whose schematics are of the same type as proposed by Yuasa *et al.* (Fig. 1).

Among the hypotheses of Table 1, No. 1 is set to simplify the flow field. Numbers 2–4 and 6 are the assumptions adopted in the theory of Marxman *et al.* Number 2 makes it possible to apply Reynolds analogy. Number 3 is

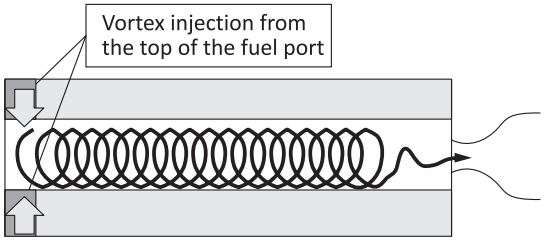

Figure 1 Schematics of swirl-injection hybrid rocket engines considered herein

declared here because the Karman's momentum integral equation is used in the authors' derivation of the friction coefficient with fuel blowing. Numbers 4 and 5 simplify the calculation of swirl numbers; moreover, in the experiments of Kito *et al.* [8] and Steenbergen [9], the flow fields substantiating these hypotheses are observed downstream where the effects of the swirlers used are small. The reason for applying the power law to the angular velocity with No. 7 is that the definition of shear stress in the radial direction parallel to the circumferential direction is expressed as $\mu r(\partial\omega/\partial r)$. Hypothesis No. 9 is adopted following the experimental results of Kito *et al.* [8] and Steenbergen [9] and to simplify the problem. In all their experimental results obtained downstream where the effects of the swirlers are small, the axial component of the boundary layer thickness is larger than the circumferential one. Number 10 is set to simplify the flow field and some researchers such as Karabeyoglu and Altman [10] have also adopted this assumption for this reason. This assumption is reasonable in swirl-injection hybrids. In the aspect of heat transfer into solid fuels, convective heat transfer is dominant in regions where turbulence in boundary layer is well developed [11]. The flow created by swirl injectors seems to be more turbulent than that induced by axial injectors. Moreover, stream lines of swirl flow are longer than those of axial flow at the same axial position, and the turbulence in the swirl flow in the boundary layer seems to be developed at a shorter axial position than that for the axial flow. However, the present authors think this assumption is not always suitable if metal or carbon powders are added to fuel to increase radiation or absorption of heat during combustion.

3 DERIVATION OF REGRESSION RATES IN SWIRL-INJECTION HYBRID ROCKET ENGINES

The aim of this section is to theoretically derive the equation for regression rates in swirl-injection hybrid rocket motors on the basis of the hypotheses discussed in the previous section. Because the regression rates are linked to the heat flux to the wall through Eq. (1) of energy conservation, in order to derive the expression for the regression rate in terms of the variables of swirl flow, let us express the heat flux to the wall using fluid dynamics and combustion considerations. Therefore, first, in the same way as Marxman *et al.*, let us try to relate the axial velocity field with the temperature field through Reynolds analogy which is extended from Lees's model in two-dimensional (2D) coordinates to the model in axisymmetric 3D coordinates. Because each radial partial differential of them is proportional to the axial components of shear stress and heat flux, respectively, it is possible to express heat flux through the flow variables in the combustion chamber (Fig. 2). Next, let us express the axial

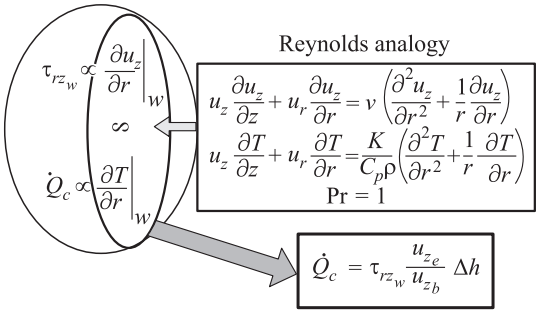

Figure 2 Reynolds analogy

shear stress through the motor scale, axial position, thermochemical and mechanical parameters of propellants, and the boundary conditions related to the flow in engine such as the swirl strength at the injectors, the axial velocity, and Reynolds number in the main flow. In the process of derivation of the axial shear stress at the wall, the present authors introduce four boundary layer models. Three of the four models are, respectively, different turbulent models in the boundary layer and the last one is the Karman's momentum integral equation. This approach is the same as the one of Marxman *et al.*, namely, it applies multiplication of the correction terms for the skin-friction coefficient in the flat-plate boundary layer without fuel blowing. The correction terms describe the effects of fuel blowing and swirl injection and are derived separately. Finally, the combination of this expression with Eq. (1) and the empirical rule for the skin-friction coefficient in 2D flat-plate boundary layer without fuel blowing makes it possible to derive the regression rates for the swirl-injection engines.

3.1 Reynolds Analogy

Reynolds analogy claims the similarity of the velocity boundary layer to the thermal boundary layer. This analogy holds because the effect of axial partial differentials in both viscosity and pressure terms is much smaller than radial partial differentials and, therefore, can be ignored in boundary layers. Let us extend this analogy to the 3D axisymmetric coordinates.

Compare the momentum equation with the energy conservation equation. The momentum equation for the axial component can be written as

$$u_z \frac{\partial u_z}{\partial z} + u_r \frac{\partial u_z}{\partial r} = \nu \left(\frac{\partial^2 u_z}{\partial r^2} + \frac{1}{r} \frac{\partial u_z}{\partial r} \right)$$

where the hypothesis No. 1 was used and it was assumed that the axial gradients of shear stress and pressure are much smaller than the radial ones as an approximation which can commonly be used in the boudary layer. The energy conservation law can be written as

$$u_z \frac{\partial T}{\partial z} + u_r \frac{\partial T}{\partial r} = \frac{K}{c_p \rho} \left(\frac{\partial^2 T}{\partial r^2} + \frac{1}{r} \frac{\partial T}{\partial r} \right)$$

where it was assumed that the effect of viscous dissipation can be ignored as compared with the convective heat transfer coming from flame. Assuming that Prandtl number is 1 (hypothesis No. 2), Reynolds analogy can be used and the temperature distribution can be related to the velocity distribution in the boundary layer. Thus, one can consider the radial distribution of u_z to be similar to that of T in the boundary layer. This similarity can be expressed as follows:

$$\frac{du_z}{u_{z_b} - u_z} = \frac{dT}{T_b - T} \,. \tag{2}$$

Then, the heat flux to the wall can be linked with the shear force stress at the wall because the axial temperature differential at the wall is proportional to the heat flux to the wall and the velocity axial differential is proportional to the shear stress at the wall. The difference between the scales of the axial and radial differentials yields the following approximations:

$$du_z \approx \frac{\tau_{rz}}{\mu} \, dr \,; \quad dT \approx -\frac{q_r}{K} \, dr \,. \tag{3}$$

Equations (2) and (3) yield

$$h \equiv -\frac{q_{r_w}}{T_b - T_w} = \frac{c_p \tau_{r z_w}}{u_{z_b}} \,. \tag{4}$$

From the definition of Stanton numbers and Eq. (4), the following equation can be derived:

$$C_H \equiv \frac{h}{c_p \rho u_b} = \frac{\tau_{r z_w}}{\rho_b u_b} \,.$$

For the sake of convenience in subsequent calculations, the nondimensional axial skin-friction parameter can be defined that is called "axial skin-friction coefficient"

$$\frac{c_{fz}}{2} \equiv -\frac{\tau_{r z_w}}{\rho_e u_{z_e}^2} \left(= -\frac{\tau_{z_w}}{\rho_e u_{z_e}^2} \right) \tag{5}$$

where the minus sign is put to show that the shear stress at the wall is always opposit to the flow direction. Therefore, the heat flux to the wall can be written as

$$\dot{Q}_c = C_H \rho_b u_b \Delta h = \frac{c_{f_z}}{2} \frac{\rho_e u_{z_e}^2}{u_{b_z}} \Delta h \,. \tag{6}$$

Let us focus on the right-hand side of Eq. (6). In this expression, there is no variable related to circumferential components. Considering the fact that the circumferential energy balance is zero because of the axisymmetric flow, this result is reasonable. Then, one can expect that the axial friction coefficient should be affected only by swirl because of the hypothesis of Marxman *et al.* [12]. Therefore, in the next section, an attempt is made to express the axial skin-friction coefficient through the axial distance, mass flux, swirl number, scale of the motor, and other variables known in advance.

3.2 Turbulent Flow Models

Next, let us express the axial skin-friction coefficient through other parameters that can be known in advance. The first of three different turbulent stress models is the Prandtl's mixing length theory extended to three dimensions by Czernuszenko and Rylov [13]. If each eigenvector of the mixing length tensor is parallel to each cylinder coordinate axis and all norms of the eigenvectors are the same, the axial component of the shear stress including Reynolds stress is expressed as

$$\tau_{rz} \approx \left\{ \mu + \rho l^2 \left(\left| \frac{\partial \overline{u}_\theta}{\partial r} - \frac{\overline{u}_\theta}{r} \right| + \left| \frac{\partial \overline{u}_z}{\partial r} \right| \right) \right\} \frac{\partial \overline{u}_z}{\partial r} \tag{7}$$

where the circumferential partial differentials are assumed to be much larger than the axial ones.

The second one comes from the expression in the boundary layer theory for the evaporating surface of flat plate in 2D coordinates extended by Dorance and Dore [14] to the 3D axisymmetric flows:

$$\tau_{rz} \approx \tau_{rz_w} \left(1 + B_z \varphi_z\right) ; \tag{8}$$

$$\tau_{r\theta} \approx \tau_{r\theta_w} \left(1 + B_\theta \varphi_\theta\right) \tag{9}$$

where the boundary layer thickness is assumed to be much thinner than the port radius. The definitions of B_z and B_θ are

$$B_z \equiv \frac{(\rho u_r)_w u_{z_e}}{\tau_{z_w}} ; \quad B_\theta \equiv \frac{(\rho u_r)_w u_{\theta_e}}{\tau_{\theta_w}} .$$

Equations (8) and (9) are derived by evaluating the Reynolds stress and blowing factor in the same way as it is made for the flat plate. Note that B_z is

constant throughout the fuel port while B_θ is not. The reason for this treatment is discussed below in subsection 3.6.

So far, two of three turbulent models have been already introduced. From now on, let us use these equations for evaluating the velocity distribution and the axial skin-friction coefficient. Combining Eq. (7) with Eq. (8) yields

$$\tau_{rz_w}\,(1+B_z\varphi_z)=\left\{\mu+\rho l^2\left(\left|\frac{\partial\overline{u}_\theta}{\partial r}-\frac{\overline{u}_\theta}{r}\right|+\left|\frac{\partial\overline{u}_z}{\partial r}\right|\right)\right\}\frac{\partial\overline{u}_z}{\partial r}\,. \tag{10}$$

Here, the power law in cases of no fuel vaporization (hypotheses Nos. 6 and 7) is written as

$$\varphi_z=\eta_z^{n_z}\,;\qquad \overline{\omega}=\eta_\theta^{n_\theta} \tag{11}$$

where $n_z=n_\theta=1/7$ is set.

Applying Eqs. (11) to the absolute values of the velocity partial differentials in Eq. (10) yields

$$\begin{aligned}\frac{c_{f_z}}{2}\,\frac{u_{z_e}(R-\delta_\theta)}{\kappa^2 n_\theta\delta_z u_{\theta_e}}\,(1+B_z\varphi_z)\\ =\left\{\eta_z^2-\frac{R-\delta_\theta}{\delta_z}\left(1+\frac{n_z u_{z_e}}{n_\theta u_{\theta_e}}\right)\eta_z-\frac{u_{z_e}(R-\delta_\theta)}{\kappa^2\mathrm{Re}_{\delta_z}n_\theta\delta_z u_{\theta_e}}\right\}\frac{\partial\varphi_z}{\partial\eta_z}\end{aligned} \tag{12}$$

where $l=\kappa(R-r)$ and $\kappa=0.4$.

Equation (12) can be integrated in the radial direction from the edge of the boudary layer to the fuel port wall. This integration yields

$$\frac{c_{f_z}}{2}\approx\frac{\kappa^2(n_\theta u_{\theta_e}/u_{z_e}+n_z)}{\ln\left(1+\kappa^2\mathrm{Re}_{\delta_z}(n_\theta u_{\theta_e}/u_{z_e}+n_z)\right)}\,\frac{\ln(1+B_z)}{B_z} \tag{13}$$

where the approximations $R\gg\delta_z,\delta_\theta$ and $\kappa^2\mathrm{Re}_{\delta_z}n_\theta\gg 1$ are used. The first term in the right-hand side of Eq. (13) can be approximated in the easier way as

$$\frac{c_{f_z}}{2}=(\alpha_z\xi+\beta_z)\,\mathrm{Re}_{\delta_z}^{\gamma_z}\,\frac{\ln(1+B_z)}{B_z} \tag{14}$$

where $(\alpha_z,\beta_z,\gamma_z)=(0.00769,0.0233,-0.125)$ is set. Let us refer $\xi\equiv u_{\theta_e}/u_{z_e}$ to as the "swirl strength." If $\xi=0$, Eq. (14) becomes the same as Marxman's approximation [6].

Though the axial skin-friction coefficient has been written as Eq. (14) through the variables descibing the flow properties, in Eq. (14), there are three variables that cannot be easily determined: ξ, u_{z_e}, and δ_z. Therefore, three additional constraints are necessary.

The first one is the Boussinesq approximation, which is the third of the three turbulent models:

$$\tau_{rz} = \frac{(\mu + \rho\varepsilon)u_{z_e}}{\delta_z} \frac{\partial \varphi_z}{\partial \eta_z} ; \tag{15}$$

$$\tau_{r\theta} = (\mu + \rho\varepsilon) \frac{u_{\theta_e}}{\delta_\theta} \frac{\partial \varphi_\theta}{\partial \eta_\theta} . \tag{16}$$

Applying Eqs. (15) and (16) to Eqs. (8) and (9) yields

$$\frac{\tau_{rz_w}\delta_z}{(\mu + \rho\varepsilon)u_{z_e}} (1 + B_z\varphi_z) = \frac{\partial \varphi_z}{\partial \eta_z} ; \tag{17}$$

$$\frac{\tau_{r\theta_w}\delta_\theta}{(\mu + \rho\varepsilon)u_{\theta_e}} (1 + B_\theta\varphi_\theta) = \frac{\partial \varphi_\theta}{\partial \eta_\theta} . \tag{18}$$

It is assumed here that $\tau_{rz_w}\delta_z/((\mu+\rho\varepsilon)u_{z_e})$ consists of the product of two single-variable functions of η_z and B_z just in the same way as in Marxman's [5]. In the cases of no blowing, Eqs. (17) and (18) are equivalent to the derivative-type of Eqs. (11). Moreover, one can use the approximation:

$$1 + B_z\varphi_z \approx 1 + B_z\eta_z^{n_z}$$

because of the hypothesis No. 6. Therefore, Eq. (17) can be expressed as

$$\frac{\partial \varphi_z}{\partial \eta_z} = F(B_z)n_z\eta_z^{n_z-1} (1 + B_z\eta_z^{n_z}) . \tag{19}$$

Equation (19) can be now integrated in the radial direction from the edge of the boudary layer to the fuel port wall. Applying the boundary conditions $\varphi_z(\eta_z = 0) = 0$ and $\varphi_z(\eta_z = 1) = 1$ leads to

$$\varphi_z = \frac{\eta_z^{n_z} (1 + (B_z/2)\eta_z^{n_z})}{1 + B_z/2} . \tag{20}$$

As for the circumferential direction, similar to the derivation of Eq. (20), one can derive

$$\overline{\omega} = \frac{\eta_\theta^{n_\theta} (1 + (B_\theta/2)\eta_\theta^{n_\theta})}{1 + B_\theta/2} \tag{21}$$

where $R \gg \delta_z, \delta_\theta$ is assumed.

Now, the velocity fields have been evaluated for the radial direction in the boundary layer. These equations are used in two situations. One of them is the case when one compares shear stresses with and without fuel blowing. Another is the case when Eqs. (14), (20), and (21) are combined to obtain the Karman's momentum integral equation and the axial skin-friction coefficient is derived as a function of axial position.

3.3 Karman's Momentum Integral Equation

Let us now derive the Karman's momentum integral equation in the axisymmetric pipe flow as the second condition for eliminating an unknown variable in Eq. (14). The mass conservation and the momentum conservation laws read:

– mass conservation law

$$\frac{\partial u_z}{\partial z} + \frac{\partial u_r}{\partial r} + \frac{u_r}{r} = 0\,; \tag{22}$$

– momentum conservation law

$$u_z \frac{\partial u_z}{\partial z} + u_r \frac{\partial u_z}{\partial r} = -\frac{1}{\rho}\frac{\partial P}{\partial z} + v\left(\frac{\partial^2 u_z}{\partial r^2} + \frac{1}{2}\frac{\partial u_z}{\partial r}\right)\,; \tag{23}$$

$$\frac{u_\theta^2}{r} = -\frac{1}{\rho}\frac{\partial P}{\partial r}\,; \tag{24}$$

$$u_z \frac{\partial u_\theta}{\partial z} + u_r \frac{\partial u_\theta}{\partial r} + \frac{u_r u_\theta}{r} = v\left(\frac{\partial^2 u_\theta}{\partial r^2} + \frac{1}{r}\frac{\partial u_\theta}{\partial r} - \frac{u_\theta}{r^2}\right)\,.$$

where axial partial differentials were ignored in viscous terms.

Equation (22) multiplied by zu_z plus Eq. (23) multiplied by r and the partial integration of Eq. (19) yield the momentum integral equation

$$\frac{\partial}{\partial z}\int_R^{R-\delta_z} r u_z^2\,dr - u_{z_e}\frac{\partial}{\partial z}\int_R^{R-\delta_z} r u_z\,dr = -\frac{R\tau_{rz_w}}{\rho}(1+B_z) - \frac{\partial}{\partial z}\int_R^{R-\delta_z}\frac{rP}{\rho}\,dr \tag{25}$$

where $(\rho u_r)_w$ must be considered as a nonzero variable. Contrary to axial flows, $\partial P/\partial r$ is approximated as 0 at the edge of boundary layer; in swirl flows, this assumption cannot be used because of Eq. (24). Thus, one should consider how to evaluate the pressure gradient $(\partial/\partial z)(rP/\rho)$. Now, the pressure in the boundary layer can be expressed as

$$P(z,r) = P(z,R-\delta_z) + \int_{R-\delta_z}^{r}\left.\frac{\partial P}{\partial r}\right|_z dr = P(z,R-\delta_z) - \int_{R-\delta_z}^{r}\rho\frac{u_\theta^2}{r}\,dr\,. \tag{26}$$

Applying Eq. (26) to the second term in the right-hand side of Eq. (25) leads to

$$\frac{\partial}{\partial z}\int_R^{R-\delta_z}\frac{rP}{\rho}\,dr = \int_R^{R-\delta_z} r\left(\frac{1}{\rho}\left.\frac{\partial P}{\partial z}\right|_{R-\delta_z} - \frac{\partial}{\partial z}\int_{R-\delta_z}^{r}\frac{u_\theta^2}{r}\,dr\right)dr\,. \tag{27}$$

The hypothesis No. 4 and Eq. (25) yield for the edge of the boundary layer:

$$\left.\frac{\partial P}{\partial z}\right|_{R-\delta_z} = 0\,. \tag{28}$$

Because of hypothesis No. 9, one can divide the last term of Eq. (27) and evaluate it as

$$\begin{aligned}
-\int_R^{R-\delta_z}\left(r\,\frac{\partial}{\partial z}\int_{R-\delta_z}^{r}\frac{u_\theta^2}{r}\,dr\right)dr &= -\frac{\partial}{\partial z}\int_{R-\delta_\theta}^{R-\delta_z} r\left(\int_{R-\delta_z}^{r}\frac{u_\theta^2}{r}\,dr\right)dr \\
&\quad -\frac{\partial}{\partial z}\int_R^{R-\delta_z} r\left(\int_{R-\delta_z}^{R-\delta_\theta}\frac{u_\theta^2}{r}\,dr\right)dr - \frac{\partial}{\partial z}\int_R^{R-\delta_\theta} r\left(\int_{R-\delta_\theta}^{r}\frac{u_\theta^2}{r}\,dr\right)dr \\
&\approx \frac{1}{2}\,\frac{\partial}{\partial z}\left\{R^2\omega_e^2\left(\delta_z^2-\delta_\theta^2\right)\right\} + \frac{\partial}{\partial z}\left\{\frac{49(170B_\theta^2+792B_\theta+935)R^2\omega_e^2\delta_\theta^2}{33{,}660(B_\theta+2)^2}\right\}
\end{aligned} \tag{29}$$

where the last expression is an approximated form of the first and the second expressions when only the largest scale terms ($\partial R^2\delta^2/\partial z$) are left. Applying Eqs. (28) and (29) to Eq. (25) and nondimensionalizing it, one obtains:

$$\begin{aligned}
&\frac{7(40B_z^2+143B_z+110)}{1980(B_z+2)^2}\,\frac{\partial\delta_z}{\partial z} \approx \frac{c_{f_z}}{2}\,(1+B_z) \\
&\quad + \frac{1}{2}\,\frac{\partial}{\partial z}\left\{\xi^2\,\frac{\delta_z^2-\delta_\theta^2}{R(1-\delta_\theta/R)^2}\right\} + \frac{\partial}{\partial z}\left\{\frac{49(170B_\theta^2+792B_\theta+935)\xi^2\delta_\theta^2}{33{,}660(B_\theta+2)^2R(1-\delta_\theta/R)^2}\right\}.
\end{aligned} \tag{30}$$

Because the order of magnitude of the last two terms in the right-hand side of Eq. (30) is $\delta^2/(RL)$ which is much smaller than the one in the right-hand side (δ/L), one can approximate Eq. (30) as

$$\frac{7(40B_z^2+143B_z+110)}{1980(B_z+2)^2}\,\frac{\partial\delta_z}{\partial z} \approx \frac{c_{f_z}}{2}\,(1+B_z)\,. \tag{31}$$

This is the Karman's momentum integral equation in the 3D axisymmetric coordinates. This equation is the last one of the four models related to boundary layers.

3.4 Estimation of the Axial Skin-Friction Coefficient in Swirl Flows with No Blowing

The aim of this subsection is to show the last of three conditions needed to evaluate the axial skin-friction coefficient. Also, an attempt will be made to evaluate this coefficient in swirl and axial flows without blowing.

Before the last condition related to swirl decay will be introduced, let us define the indicator which shows the swirl strength. The swirl number is a way to express the swirl strength as:

$$S \equiv \frac{2}{R^3 u_{z_e}^2} \int_0^R r^2 u_z u_\theta \, dr \, .$$

Considering the hypotheses Nos. 4 and 5 and ignoring boundary layers, rough calculation yields

$$S \approx \frac{\xi}{2} \, .$$

Here, ξ is called "swirl strength." The last condition is the hypothesis No. 8 with the mathematical manifestation as

$$S \approx S_0 \exp(pz) \;\text{ or }\; \xi \approx \xi_0 \exp(pz) \tag{32}$$

where $p = -0.569 \mathrm{Re}_D^{-0.277}/D$. These equations are empirically derived from Kito *et al.* [8] and Steenbergen [9].

Now, necessary and sufficient conditions have been assembled which are Eqs. (20), (21), (31), and (32), to rewrite Eq. (14) as a single-variable function of axial direction. Next, let us compare and evaluate c_{f_z} for the case without blowing and swirling, namely, evaluate c_{f_z} as

$$\left.\frac{c_{f_z}}{2}\right|_{B_z,\xi_0} = \frac{c_{f_z}|_{B_z,\xi_0}}{c_{f_z}|_{B_z=0,\xi_0}} \frac{c_{f_z}|_{B_z=0,\xi_0}}{c_{f_z}|_{B_z=0,\xi_0=0}} \left.\frac{c_{f_z}}{2}\right|_{B_z=0,\xi_0=0} \tag{33}$$

where $(c_{f_z}/2)|_{B_z=0,\xi_0=0}$ is equivalent to $c_f/2$ in the cases of 2D flat plate and $c_f/2$ follows a famous empirical rule:

$$\frac{c_f}{2} = 0.03 \mathrm{Re}_z^{-0.2} \, . \tag{34}$$

In this subsection, $c_{f_z}|_{B_z=0,\xi_0}/c_{f_z}|_{B_z=0,\xi_0=0}$ will be evaluated for the initial swirl strength and axial direction. Now, for the cases without blowing, substituting Eqs. (14) and (32) into Eq. (31) and integration of Eq. (31) in the axial direction from 0 to z yield

$$\overline{\delta}_z|_{B_z=0} = \left\{ \frac{72(1-\gamma_z)}{7} \right\}^{1/(1-\gamma_z)} \mathrm{Re}_D \left(\alpha_z \xi_0 \frac{\exp(\overline{p}\,\overline{z}) - 1}{\overline{p}} + \beta_z \overline{z} \right)^{1/(1-\gamma_z)} \tag{35}$$

where the bar means that the variable is nondimensionalized by the port diameter. By substituting Eq. (35) into Eq. (31) and dividing Eq. (31) with swirl by the one without swirl, one obtains

$$\frac{c_{f_z}|_{B_z=0,\xi_0}}{c_{f_z}|_{B_z=0,\xi_0=0}} = \frac{c_{f_z}/2|_{B_z=0,\xi_0}}{c_f/2}$$
$$= \left(\frac{\alpha_z}{\beta_z}\,\xi_0\,\frac{\exp(\overline{p}\,\overline{z})-1}{\overline{p}\,\overline{z}}+1\right)^{1/(1-\gamma_z)}\left(\frac{\alpha_z}{\beta_z}\,\xi_0\exp(\overline{p}\,\overline{z})+1\right). \quad (36)$$

Equation (36) shows the relation between the axial skin-friction coefficient with swirl but without fuel blowing. This evaluation is used in the next subsections.

3.5 Estimation of the Axial Friction Coefficient in Swirl Flows with Blowing

In this subsection, let us start from comparing shear stresses with and without fuel blowing. Then, let us express the boundary layer thickness and the axial skin-friction coefficient through the fuel blowing and axial blowing parameter.

First of all, let us write the shear stress at the wall with fuel blowing as

$$\tau_{rz_w}|_{B_z} = \mu\,\frac{u_{z_e}}{\delta_z|_{B_z}}\left.\frac{\partial\varphi_z}{\partial\eta_z}\right|_w. \quad (37)$$

Near the wall, nondimensional axial velocity is approximated as follows:

$$\varphi_z = \frac{\eta_z^{n_z}\,(1+(B_z/2)\,\eta_z^{n_z})}{1+B_z/2} \approx \frac{\eta_z^{n_z}}{1+B_z/2}. \quad (38)$$

Substituting Eq. (38) into Eq. (37) yields

$$\tau_{rz_w}|_{B_z} \approx \frac{\mu}{1+B_z/2}\,\frac{u_{z_e}}{\delta_z|_{B_z}}\left.\frac{\partial\eta_z^{n_z}}{\partial\eta_z}\right|_w = \frac{1}{1+B_z/2}\,\frac{\delta_z|_{B_z=0}}{\delta_z|_{B_z}}\;\tau_{rz_w}|_{B_z=0}. \quad (39)$$

Therefore, Eq. (39) can be nondimensionalized as

$$\left.\frac{c_{f_z}}{2}\right|_{B_z} = \frac{1}{1+B_z/2}\,\frac{\delta_z|_{B_z=0}}{\delta_z|_{B_z}}\left.\frac{c_{f_z}}{2}\right|_{B_z=0}. \quad (40)$$

Applying Eq. (31) to the both sides of Eq. (40) and integration in the axial distance yield

$$\delta_z|_{B_z} = \sqrt{\frac{(1+B_z)(1+B_z/2)}{1+(13/11)B_z+(4/11)B_z^2}}\;\delta_z|_{B_z=0}. \quad (41)$$

By substituting Eq. (41) into Eq. (31) and approximating B_z in the range from 2 to 50, one obtains

$$\frac{c_{f_z}|_{B_z}}{c_{f_z}|_{B_z=0}} = \frac{1}{1+B_z/2}\sqrt{\frac{1+(13/11)B_z+(4/11)B_z^2}{(1+B_z)(1+B_z/2)}} \approx q' B_z^{-k'} \tag{42}$$

where $(q', k') = (0.7275, 0.965)$.

Combining Eq. (33) with Eqs. (34), (36), and (42), one can evaluate the axial skin-friction coefficient as

$$\left.\frac{c_{f_z}}{2}\right|_{B_z} = \left(\frac{\alpha_z}{\beta_z}\,\xi_0\,\frac{\exp(\overline{p}\,\overline{z})-1}{\overline{p}\,\overline{z}}+1\right)^{1/(1-\gamma_z)} \times \left(\frac{\alpha_z}{\beta_z}\,\xi_0\exp(\overline{p}\,\overline{z})+1\right) q' B_z^{-k'}\cdot 0.03\mathrm{Re}_z^{-0.2}\,. \tag{43}$$

3.6 Derivation of Regression Rates in Swirl Injection Engines

In the previous subsection, the axial skin-friction coefficient was derived for conditions with swirl and fuel blowing as Eq. (41). The aim of this subsection is to obtain the heat flux to the wall and the regression rates in swirl hybrids. Now, substituting Eq. (6) into Eq. (43) yields

$$\dot{Q}_c = (0.03q')^{1/(1-k')}\,\rho_f^{-k'/(1-k')}\Delta h\,\frac{u_{z_e}}{u_{z_b}}\left(\frac{z}{\mu}\right)^{-0.2/(1-k')} \times \left(1+\frac{\alpha_z}{\beta_z}\,\xi_0\,\frac{\exp(pz)-1}{pz}\right)^{\gamma_z/((1-\gamma_z)(1-k'))} \left\{1+\frac{\alpha_z}{\beta_z}\,\xi_0\exp(pz)\right\}^{1/(1-k')} \times G_{zo}^{0.8/(1-k')}\dot{r}^{-k'/(1-k')} \tag{44}$$

where B_z has been eliminated with the definition of B_z and Eq. (43).

Substituting Eq. (44) into Eq. (1) yields

$$\dot{r} = \left(1+\frac{\alpha_z}{\beta_z}\,\xi_0\,\frac{\exp(pz)-1}{pz}\right)^{\gamma_z/(1-\gamma_z)} \times \left\{1+\frac{\alpha_z}{\beta_z}\,\xi_0\exp(pz)\right\} 0.03q'\left(\frac{z}{\mu}\right)^{-0.2}\rho_f^{-1}B_t^{1-k'}G_{zo}^{0.8} \tag{45}$$

where the definition of B_t is

$$B_t \equiv \frac{u_{e_z}\Delta h}{u_{b_z}h_\nu}$$

and B_t is equivalent to B_z at quasi-steady states because of Eqs. (1) and (6). Because B_t is a function of the thermochemical properties and O/F [12] when O/F is constant, B_t is constant in axial and radial directions. This is the reason why B_θ is considered as a variable and B_z as a constant.

According to the results by Marxman *et al.* [12], the heat flux to the wall can be expressed as follows:

$$\dot{Q}_c = (0.03q)^{1/(1-k)} \rho_f^{-k/(1-k)} \Delta h \, \frac{u_e}{u_b} \left(\frac{z}{\mu} \right)^{-0.2/(1-k)} G_o^{0.8/(1-k)} \dot{r}^{-k/(1-k)} \,. \quad (46)$$

Therefore, Eqs. (1) and (46) yield

$$\dot{r} = 0.03q \left(\frac{z}{\mu} \right)^{-0.2} \rho_f^{-1} B_t^{1-k} G_o^{0.8} \,. \quad (47)$$

Note that the experimental law for the regression rate is as follows:

$$\dot{r} = a \; G_o^n \,. \quad (48)$$

According to Karabeyoglu's theory [15], in axial flows, averaging of Eq. (47) in axial direction is equivalent to Eq. (48) and the exponent 0.8 at G_o in Eq. (47) should correspond to the exponent n at G_o in Eq. (48). On the basis of these findings, the coefficient a in Eq. (48) should be

$$a_0 = 0.03q \left(\frac{z}{\mu} \right)^{-0.2} \rho_f^{-1} B_t^{1-k} \quad (49)$$

where a is replaced by a_0 and $(q, k) = (1.2, \; 0.77)$ [6]. Then, in the same way as in Eq. (49), a in Eq. (45) should be equal to

$$a_\xi = \left(1 + \frac{\alpha_z}{\beta_z} \, \xi_0 \, \frac{\exp(pz) - 1}{pz} \right)^{\gamma_z/(1-\gamma_z)} \times \left\{ 1 + \frac{\alpha_z}{\beta_z} \, \xi_0 \exp(pz) \right\} 0.03q' \left(\frac{z}{\mu} \right)^{-0.2} \rho_f^{-1} B_t^{1-k'}$$

where a is replaced by a_ξ. These two coefficients show how the regression rates rise with the initial swirl strength ξ_0:

$$\frac{\dot{r}_\xi}{\dot{r}_0} = \frac{a_\xi}{a_0} = \left(1 + \frac{\alpha_z}{\beta_z} \, \xi_0 \, \frac{\exp(pz) - 1}{pz} \right)^{\gamma_z/(1-\gamma_z)} \left\{ 1 + \frac{\alpha_z}{\beta_z} \, \xi_0 \exp(pz) \right\} \frac{q'}{q} \, B_t^{k-k'} \,. \quad (50)$$

Thus, the heat flux to the wall and regression rates in swirl flows have been estimated.

4 COMPARISON OF THE REGRESSION RATES OF SWIRL ENGINES WITH EXPERIMENTS

In order to validate the model, one can compare the increase of the regression rate by swirl predicted by Eq. (50) and obtained in experiments by Yuasa *et al.* [3]. In this section, the prediction of Eq. (50) will be compared with the experiments in two ways. One of them is the comparison between the representative regression rates in the axial direction with space averaged values of the experimental results. Another one is the comparison of the axial distributions of regression rates.

4.1 Comparison of Representative and Averaged Regression Rates Along the Axial Direction

The fuel and oxidizer used in Yuasa's experiments are polymethylmethacrylate (PMMA) and gaseous oxygen. For PMMA [16], $B_t = 10$ and $\mu = 5.0 \cdot 10^{-7}$ Pa·s were set. To compare the prediction with the averaged data, let us set the representative axial location in Eq. (50) as $L/2$. The geometric swirl numbers of the injectors are 0, 9.7, and 19.4 and the range of the oxidizer mass flux is from 10 to 70 kg/(m^{2}s). The case with the port length $L = 150$ mm is shown in Fig. 3 and that with $L = 500$ mm is shown in Fig. 4.

In Yuasa's experiments, they claimed it was too difficult to measure the actual swirl numbers in their motors and when they plotted the regression rates, they used a kind of index called geometric swirl number indicating the strength of the swirl. This index is determined only by the geometry of engines and injectors and

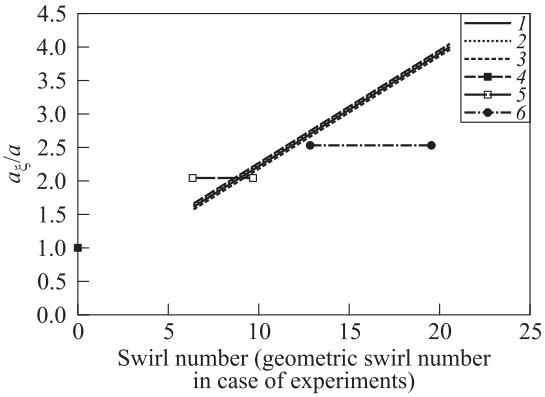

Figure 3 The ratio of constant a in swirl hybrid rocket engines for $L = 150$ mm: *1* — $G_o = 10$ kg/(m^{2}s); *2* — 15; *3* — $G_o = 20$ kg/(m^{2}s); *4* — experiment-1; *5* — experiment-2; and *6* — experiment-3

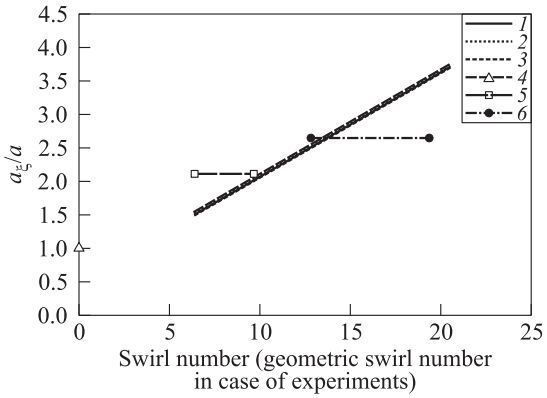

Figure 4 The ratio of constant a in swirl hybrid rocket engines for $L = 500$ mm: *1* — $G_o = 45$ kg/(m^{2}s); *2* — 50; *3* — $G_o = 55$ kg/(m^{2}s); *4* — experiment-1; *5* — experiment-2; and *6* — experiment-3

the authors think this number is not always equal to the actual swirl number. As a matter of fact, Motoe and Shimada [17] conducted numerical simulations of the swirl cold flow field where they used the shape or geometry of the chamber similar to Yuasa's. The calculated swirl numbers near the injectors were 0.66 in condition that the geometric swirl number was 5.5. For this reason, the present authors plotted the regression rate in Yuasa's experiment with the error bar in the swirl number direction. The error bars have the range of 66% to 100% of the geometry swirl numbers.

Note that for both port lengths, at large swirl numbers, the increase in the regression rates is largely consistent with the experiments and the positive correlation between the initial swirl numbers and the increase in the regression rates also generally exist in the set of experimental results and in the present authors' predictions. In their past research, because the present authors assumed that the decay of swirl and the axial skin-friction are not affected by fuel blowing, the increase in the regression rate was estimated to be much larger than in the experiments [18]. In this paper, this assumption was reconsidered because it does not reflect the actual physical phenomena as the swirl decay is mainly caused by skin-friction at the wall and fuel blowing should strongly affect it. Then, the methods to evaluate the skin friction with fuel blowing have been newly considered and the approaches used in subsections 3.4 and 3.5 showed better results than the past one. Thus, the regression rates were successfully evaluated for the cases with strong swirl.

However, in the range of small swirl numbers under 3, the regression rates appeared to be less than 1. This seems to be caused by the adopted simplifications, in particular, by the assumption on the exponential decay of swirl in cold

flow and by separate consideration of the effects of swirl flow and fuel blowing on the skin-friction coefficient. However, when applying vortex injection to hybrids, the initial swirl numbers will be designed to increase the regression rate and, by authors' opinion, this estimation method will be useful.

4.2 Comparison of the Axial Distribution of Regression Rates

Next, let us compare the prediction of the local regression rates in the swirl injection hybrids with the experiments conducted by Yuasa *et al.* The geometric swirl numbers of the injectors are 0, 9.7, and 19.4 and the axial location where the local regression rates are measured is from 30 to 500 mm; the oxidizer mass flux is 56.9 kg/(m^{2}s).

Figure 5 compares the local regression rate for axial injection obtained by Eq. (47) and in the experiment. In the experimental data, while the local regression rate decreases from the front edge of the fuel port to the middle of the fuel port and increases towards the end, the predicted regression rate by Marxman's evaluation gradually decreases along the axial distance. Furthermore, the location where the prediction agrees with the experimental data is only around the local minimun position. In the present authors' opinion, this disagreement suggests that other effects which increase the regression rate such as radiation and the increase of the mass flux due to fuel blowing have to be considered.

In Fig. 6, the local regression rates predicted by Eq. (45) are compared with Yuasa's experiments for the swirl-injection hybrid mortors. Similar to the case of axial injection, while both predicted regression rates and experimental results are of the same order of magnitude for high swirl numbers, their values are not the same. As in the case of comparison of the averaged rates, especially, at low

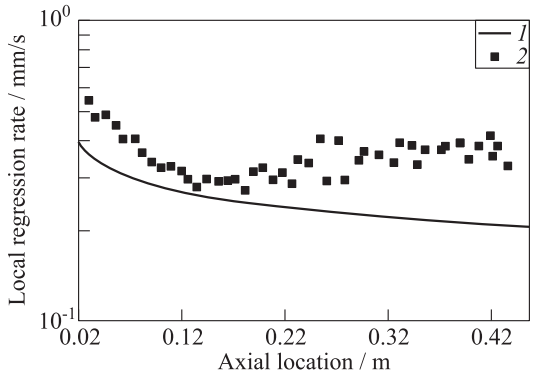

Figure 5 Comparison of the regression rates in axial hybrids between the Marxman's prediction method (*1*) and the Yuasa's experiment (*2*)

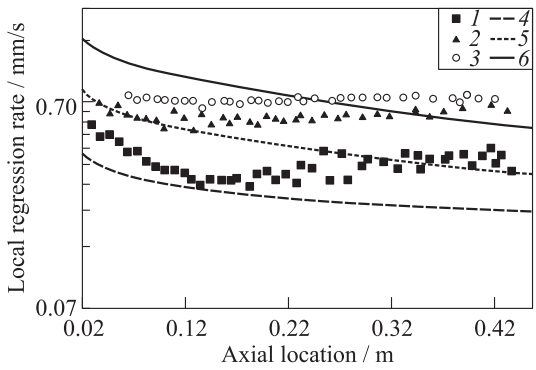

Figure 6 Comparison of the regression rates in swirl hybrids between the present theoretical prediction (curves) and the Yuasa's experiments (signs): *1* — $\xi_0 = 0$; *2* — 19.4; *3* — $\xi_0 = 38.8$; *4* — axial; *5* — $\xi_0 = 19.7 \cdot 0.66$; and *6* — $\xi_0 = 38.8 \cdot 0.66$

swirl numbers, the predictions differ considerably from the experimental data because Eq. (50) provides values under 1. Moreover, from Fig. 6, one can understand that even in the cases of axial injection where Marxman's model is thought to be applicable, the predictions of the regression rates do not agree with the experimental data and only the spatially averaged prediction agrees with the corresponding experimental data. However, according to Chiaverini *et al.* [11], the radiation effect is weakened by developing turbulence in boundary layers. In swirl flow, because streamlines near the wall are longer than in the axial flow, turbulence in the boundary layer is supposed to develop earlier and the effects of radiation should be low in swirl flow. Nevertheless, the discrepancy between theoretical and experimental regression rates does not become narrower for different swirl numbers. This consideration indicates that there exist a different mechanism of swirl number decline or the effects of fuel mass addition are large.

In view of it, before focusing on improving the evaluation of the effects caused by swirl injection, the present authors plan to use more accurate prediction models than the Marxman's classical one for predicting the distribution of local regression rates in axial flows which will consider the effect of the increase in the mass flow because of fuel vaporization.

As for the accuracy of estimating the effects of swirl, it is necessary to reconsider the relation of actual swirl numbers to the geometric ones. On the one hand, in the axial flow with swirl strength $\xi_0 = 19.4$, the predicted result is close to the experiment only around the front of fuel port; on the other hand, at $\xi_0 = 38.8$, the best agreement shifts to the middle of fuel port. In the authors' opinion, this is due to the fact that the swirl number of 0.66 is only applied to low swirl flows. In these studies, the swirl number of 0.66 has been used based

on the Motoe and Shimada numerical calculations [17]. However, this number is the result of condition that the geometric swirl number is 5.5 ($\xi_0 = 11$) and in higher swirl flows, the actual swirl numbers can decrease. In particular, in cases of high swirl strength, it is reasonable that this swirl number may not be used. Therefore, it is necessary to study the relation between actual and geometric swirl numbers.

5 CONCLUDING REMARKS

In this paper, the authors have theoretically reconstructed and extended Marxman's quasi-steady boundary layer combustion model and the prediction method for regression rates in swirling hybrid rocket motors. This has been made by extending the 2D flat-plate boundary layer theory to the 3D axisymmetric theory. The derived heat flux equation includes the effect of initial swirl strength and the swirl-strengthened fuel blocking effect. The blocking exponent for strong swirl injection is calculated to be 0.965 in contrast to 0.77 for axial injection. By using this heat flux, eventually, the equation to evaluate the regression rate in swirling hybrid rocket motors has been derived.

To confirm the accuracy of this method, the predicted results were compared with the experiments by Yuasa *et al.* in two ways. In the first, the representative increase of the regression rates by swirl in the axial direction were compared with the averaged regression rates from the experiments. Though the assumed flow field seems to be different from the experiments to some extent, the estimated regression rates are of the same order of magnitude at all swirl strengths and fit especially well at strong swirls. In the second, the predicted local regression rates were compared with experimental data from Yuasa *et al.* for both axial and swirl flows. The prediction of the classical Marxman's theory for axial injection motors was compared with the data for axial flow and the results were of the same order of magnitude, however, not accurate enough to claim the regression rates can be predicted to know the detailed performance. In the authors' opinion, the reason for this disagreement is that other effects which increase regression rates such as radiation and the increase of the mass flux by fuel blowing or other mechanisms inherent in swirl injection hybrid rocket engines have to be considered, though the radiation effect can be weakened at high swirl numbers. In swirl injection, because the theory derived in this paper is based on the classical theory of Marxman *et al.*, the accuracy of the prediction is also low. Therefore, to improve the prediction of the local regression rates in swirl injection hybrid motors, one should provide some theoretical correction of Marxman's boundary layer combustion model. Compared with experimental results, the predicted regression rates of $\xi_0 = 38.8$ were found to shift higher than the ones at low swirl num-

bers. This is because the relation of actual swirl numbers to the geometric ones can decrease due to the increase of geometric swirl numbers and it is necessary to reconsider the value of this relation at higher geometric swirl numbers.

ACKNOWLEDGMENTS

This research is supported by the Hybrid Rocket Research Working Group (HRrWG) of the Institute of Space and Astronautical Science, Japan Aerospace Exploration Agency. The authors thank the members of HRrWG for their helpful discussion.

REFERENCES

1. Zilliac, G., and M. A. Karabeyoglu. 2006. Hybrid rocket fuel regression rate data and modeling. AIAA Paper No. 2006-4504.
2. Knuth, W. H., M. J. Chiaverini, J. A. Sauer, and D. J. Gramer. 1998. Solid-fuel regression rate behavior of vortex hybrid rocket engines. *J. Propul. Power* 18:600–609.
3. Yuasa, S., K. Yamamoto, H. Hachiya, K. Kitagawa, and Y. Oowada. 2001. Development of a small sounding hybrid rocket with a swirling-oxidizer-type engine. AIAA Paper No. 2001-3537.
4. Yoshizawa, A., H. Abe, H. Fujiwara, Y. Mizobuchi, and Y. Matsuo. 2009. Reynolds-averaged modeling of turbulent-diffusion suppression mechanism in a swirling flow. *41st Fluid Dynamics Conference / Aerospace Numerical Simulation Symposium Proceedings*. 23–26.
5. Marxman, G. A., and M. Gilbert. 1963. Turbulent boundary layer combustion in the hybrid rocket. *Symposium (International) on Combustion Proceedings*. 9:371–383.
6. Marxman, G. A. 1965. Combustion in the turbulent boundary layer on a vaporing surface. *Symposium (International) on Combustion Proceedings*. 10: 1337–1349.
7. Lees, L. 1958. Convective heat transfer with mass addition and chemical reactions. *3rd AGARD Combustion and Propulsion Colloquium Proceedings*. 451.
8. Kito. M., H. Fujiwara, and K. Nakabayashi. 1985. The direct measurement of the shear stresses in swirl pipe flows. *Trans. Japan Soc. Mech. Eng. B* 51:2597–2605.
9. Steenbergen, W. 1995. Turbulent pipe flow with swirl. University Eindhoven of Technology. Ph.D. Thesis.
10. Karabeyoglu, M. A., and D. Altman. 1997. Transient behavior in hybrid rockets. AIAA Paper No. 97-2937.

11. Chiaverini, M. J., N. Serin, D. K. Johnson, Y.-C. Lu, K. K. Kuo, and G. A. Risha. 2000. Regression rate behavior of hybrid rocket solid fuels. *J. Propul. Power* 16:125–132.
12. Marxman, G. A., C. E. Wooldridge, and R. J. Muzzy. 1963. Fundamentals of hybrid boundary layer combustion. AIAA Paper No. 63-505.
13. Czernuszenko, W., and A. A. Rylov. 2000. A generalization of Prandtl's model for 3D open channel flows. *J. Hydraul. Res.* 38:173–383.
14. Dorrance, W. H., and F. J. Dore. 1954. The effect of mass transfer on the compressible turbulent boundary-layer skin friction and heat transfer. *J. Aeronaut. Sci.* 21:404–410.
15. Karabeyoglu, M. A., and D. Altman. 1999. Dynamic modeling of hybrid rocket combustion. *J. Propul. Power* 15:562–571.
16. Marxman, G. A. 1967. Boundary-layer combustion in propulsion. *Symposium (International) on Combustion Proceedings*. 11:269–289.
17. Motoe, M., and T. Shimada. 2009. Head-end injected swirling gas flow in a chamber. AIAA Paper. 2009-5025.
18. Ozawa, K., and T. Shimada. 2013. A theoretical study in the skin-friction coefficient in swirl pipe flows. *ISAS Proceedings of Space Propulsion Symposium FY2012. STCP-2012-070.* (In Japanese.)